# Beyond Turnover Time: Constraining the Lifetime Distribution of Water Vapor from Simple and Complex Approaches

HARALD SODEMANN

*Geophysical Institute, University of Bergen, and Bjerknes Centre for Climate Research, Bergen, Norway*

(Manuscript received 30 November 2018, in final form 2 October 2019)

ABSTRACT

The time water vapor spends in the atmosphere from evaporation to precipitation, termed here the water vapor lifetime, is of fundamental relevance for characterizing the water cycle, for the turnover of mass and energy, causes of precipitation extremes, and the recycling of precipitation over land. While the global average lifetime of water vapor is commonly considered as about 8–10 days, recent work indicates that the distribution of water vapor lifetimes is highly skewed, and that a large part of the water vapor could have average lifetimes of about 4–5 days. Besides calling for scrutiny of these new estimates, these findings also prompt an investigation of the factors shaping the distribution of the lifetime of water vapor. Using idealized setups and reanalysis data, I explore the influence of heterogeneity and nonstationarity on water vapor age and lifetime. The combination of nonstationarity and heterogeneity allows for short and long local lifetimes and water vapor ages, while maintaining the global average mass balance and corresponding mean water vapor lifetime. A plausibility argument based on humidity-weighted winds suggests that median lifetimes of 4–5 days are more consistent with weather system patterns in the extratropics. I propose that the median of the lifetime is more representative, since its mean value is affected by uncertainty originating from a long, thin tail. To more comprehensively understand the water vapor lifetime, methods will need to report the full lifetime distribution. Simulations with artificial water tracers could thereby provide the framework to compare different methods consistently in the future, while stable water isotopes could serve as an observational constraint.

## 1. Introduction

Water in the atmosphere is key for many feedbacks in the climate system. The atmospheric water reservoir is continuously depleted and replenished by precipitation and evaporation. A fundamentally relevant quantity of this system is the actual time that water molecules spend in the atmosphere between evaporation and precipitation, termed here the *atmospheric lifetime of water vapor*, or simply *lifetime*, often also referred to as the residence time of water vapor (Trenberth 1998). Being related to the rate of energy transformations and water mass turnover in the climate system, this atmospheric lifetime provides important insight into the time lags and linkages between processes. Examples are the conversion of energy to latent heat, and its subsequent release during condensation, or the link between a precipitation event and the contributing evaporation sources.

The age of the water when it returns to the ground as precipitation cannot be observed directly. Therefore, indirect methods have long been used to calculate an estimate of the lifetime. Traditionally, the lifetime has been estimated by a *turnover time*, mathematically equivalent to a decay-time constant of a time-averaged or stationary process that depletes and recharges the atmospheric water reservoir by the fluxes precipitation and evaporation. Using the radiosonde network and gridded precipitation data, Peixóto and Oort (1983) inferred a global average turnover time on the order of 8–10 days. This numeric value has long been used as a guiding rail for the time water vapor on average spends in the atmosphere between evaporation and precipitation (Laederach and Sodemann 2016, henceforth LS16).

Denotes content that is immediately available upon publication as open access.

*Corresponding author*: Harald Sodemann, harald.sodemann@uib.no

DOI: 10.1175/JAS-D-18-0336.1

This article is licensed under a Creative Commons Attribution 4.0 license (http://creativecommons.org/licenses/by/4.0/).

© 2020 American Meteorological Society



Unauthenticated | Downloaded 04/22/25 10:51 AM UTC

In other scientific fields than atmospheric sciences, for example, in hydrology and ecology, turnover times of systems and reservoirs have received more detailed attention (Dettmann 2013). In limnology, for instance, the systems under consideration can be lake reservoirs with or without stratification, where the inflow from tributary rivers and the outflow allow to calculate a turnover time for a system in steady state. Catchment hydrology considers the flow through a porous medium characterized by retention times that depend on the media, pore size and preferential flow paths, stagnant zones, and nonstationary input from precipitation (McGuire and McDonnell 2006).

A further analogous system can be found regarding soil organic matter (H. Tang 2018, personal communication; Trumbore 2000). Soil organic matter consists of both long-lived and short-lived carbon pools, which degrade at different rates. Some materials are decomposed within several years, whereas other components may be more than 1000 years old. The flux of $CO_2$ into the atmosphere from the soil is strongly biased toward the more short-lived components. Methods that consider the bulk carbon stock as homogeneous then underestimate the short-term response and overestimate long-term response of carbon in soils to perturbations (Trumbore 2000). While the analogy to the water cycle is limited, this example highlights that characterizing a system that is dominated by heterogeneity of reservoirs and fluxes by a single number for the lifetime can be misleading.

The atmosphere has characteristics that are quite different to the previously mentioned systems. Filled by a stratified gaseous medium where pressure and density decrease exponentially with height, water vapor behaves as a tracer variable with temperature and pressure-dependent phase-change processes during recharge and depletion. Obtaining the lifetime of water vapor in the atmosphere may require attention to such specific characteristics when concepts from hydrology or ecology are utilized.

Given the different climatic zones, distribution of land and ocean, atmospheric stratification, and the resulting weather systems, one can anticipate the lifetime of water vapor to vary between regions and with time. Stratospheric water vapor, for example, can remain without precipitation for a long time, whereas tropical convection turns over large amounts of water vapor on a diurnal basis. A desirable goal is therefore to access the full probability density function of the atmospheric lifetime of water vapor for any desired region or time interval, rather than just a single turnover time. As the lifetime of water in the atmosphere is strongly influenced by processes below the grid scale of current global weather prediction and climate models, involving a combination of radiative, microphysical, thermodynamic, and dynamic processes, and in the virtual absence of observational constraints, this aim may at least be challenging to achieve, even with currently available numerical tools.

When obtained from the hydrologic state of climate model and reanalysis data, turnover times are commonly lower than from observations, suggesting that the water cycle in models is too intense (e.g., Trenberth 1998, 2011). Held and Soden (2006) show that with increasing greenhouse gas concentrations, atmospheric water mass increases more rapidly than precipitation in climate models. According to their results, the relative increase in water mass causes a slowdown of the atmospheric water cycle, reflected by an increased turnover time. Hodnebroug et al. (2019) used the turnover time to characterize changes in the water cycle of future climate simulations. Interpretation of the changes was, however, not straightforward, possibly reflecting both amplification and slowdown of different aspects of the water cycle. As observational benchmarks are almost absent (Aggarwal et al. 2012), the turnover time appears so far as the most long-standing tool to inform about the global average lifetime of water vapor. Using turnover time as a measure to assess the fidelity of models requires that the quantity faithfully represents the full distribution of water vapor lifetimes, an aspect that has so far not been investigated in detail. One aim of this study is to explore aspects that contribute to spread in the distribution of water vapor lifetimes, and how different methods can inform about the properties of the lifetime distribution.

LS16 compared current and new estimates of the lifetime (residence time in their terminology) from different methods. They emphasized the relevance of horizontal water transport as a part of the turnover of water in the atmosphere, a factor that had so far been neglected from local turnover time calculations. From calculations of the local turnover time with a moisture transport term, they obtained estimates with more plausible spatial patterns of the lifetime than had been obtained previously. However, being intended as a broad-brush metric for the time scale, the validity of such turnover time calculations at the gridpoint level may be contested.

Using a new approach to calculate the atmospheric lifetime based on a moisture tracking algorithm using Lagrangian backward trajectories, LS16 then obtained similar spatial patterns as for the local depletion time, providing a global average of about 4–5 days, about half of the 8–10 days assumed generally. This discrepancy to the traditional estimates of the average lifetime highlighted the need to thoroughly investigate what aspect the turnover time actually measures for the atmospheric

Unauthenticated | Downloaded 04/22/25 10:51 AM UTC

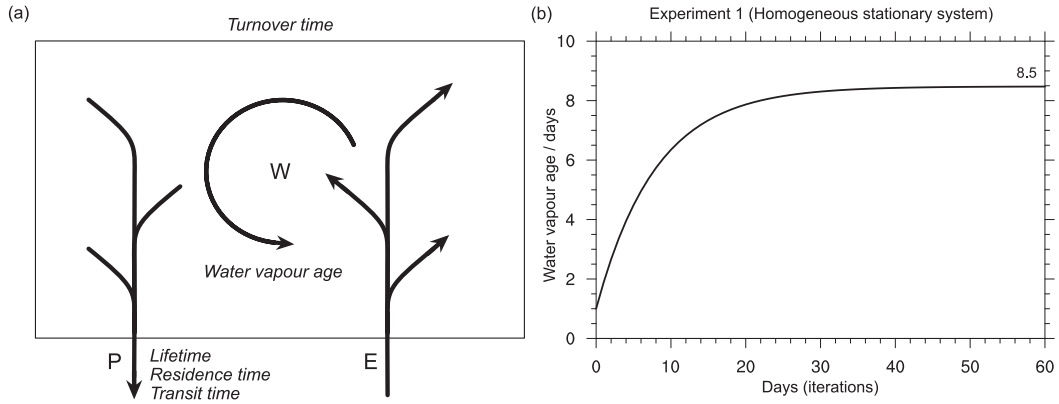


FIG. 1. Water vapor age and lifetime calculation for a homogeneous, stationary system. (a) Illustration of the budget of the atmospheric water content $W$ with flux components evaporation $E$ and precipitation $P$. Feathered arrows indicate that it is equally likely to have contributions from all parts of the atmosphere, i.e., a homogeneous, well-mixed system. (b) Evolution of the water vapor age for the homogeneous, stationary system (Experiment 1) using Eq. (2). The age stabilizes at 8.5 days after about 40 iterations. In the homogeneous system, water vapor age is equal to the lifetime.

system, while also prompting additional scrutinizing of LS16's method. The results of the Lagrangian lifetime estimates by LS16 were disputed by van der Ent and Tuinenbourg (2017, henceforth VT17), who argued that the turnover time obtained from mass balance is a reliable indicator of the mean atmospheric lifetime that would allow to reject results that substantially deviate from a numerical value of 8–10 days. As will be shown in this manuscript, this dispute can largely be resolved by considering what aspect of the full distribution of lifetimes different methods capture.

Resolving this dispute on the apparent discrepancy between the Lagrangian lifetime estimates and turnover time constants constructively is highly relevant, for example, for the widely applied method by Stohl and James (2004) to identify moisture sources from an $E$–$P$ budget along Lagrangian backward trajectories. That method requires information on the local lifetime to decide on how long precipitation should be traced back to its evaporation sources (Stohl et al. 2005; Gimeno et al. 2012). Results and interpretation of that method will differ strongly when using either the global average turnover time or the Lagrangian lifetime estimate of LS16.

In this study, I conduct an in-depth analysis of different age properties in different idealized representations of the atmospheric water cycle. I develop a framework for analyzing the atmospheric system by partitioning it into several compartments to represent inhomogeneity, and time-variant fluxes to represent nonstationarity. Considering the age of water vapor and precipitation separately will then provide a basis for understanding salient characteristics of the full distribution of the lifetime. A simple plausibility argument is applied that underlines the value of considering metrics that are more representative of the majority of the lifetime distribution than the turnover time. Throughout the manuscript, I use ERA-Interim (Dee et al. 2011) as an internally consistent database. In the final sections, I update the results from LS16 with uncertainty estimates and review currently used methods in the literature regarding their uncertainties, before closing with recommendations for a way forward to represent and obtain full distributions of water vapor lifetime.

### *a. Definitions and scope*

As a foundation to the structure of this analysis, I summarize here some key definitions (see also Fig. 1). The atmospheric lifetime of water vapor is the true quantity of the elapsed time that a water molecule has spent in the atmosphere when it returns as precipitation to the surface. Other studies refer to this quantity as the residence time, and in particular in catchment hydrology, this is sometimes referred to as the transit time of the system (McGuire and McDonnell 2006). The *water vapor age* is defined as the elapsed time, or age of all water vapor that resides in the atmosphere at a specific time. The mean water vapor age and the mean lifetime are not necessarily identical, and depend on the flow properties of a system. For example, in a steady-state pipe flow, the age of the water in the system is half the transit time, whereas in a well-mixed (homogeneous) system in steady state, the lifetime is a sample of the average water vapor age. Finally, the *turnover time* of water vapor in the atmosphere is given by the ratio between the reservoir size and the precipitation flux, and

Unauthenticated | Downloaded 04/22/25 10:51 AM UTC

TABLE 1. Characteristics of the water cycle obtained from daily ERA-Interim data for the year 2015. Values plus and minus one standard deviation calculated from daily values are provided for the global average and for zonal averages for three regions—tropics, subtropics, and extratropics—that divide Earth's surface area into equal thirds.

| Region | $W$ ($10^{15}$ kg) | $W$ (%) | IWV (kg m$^{-2}$) | Area (%) |
|---|---|---|---|---|
| Global | 12.8 ± 0.57 | 100 ± 0 | 25.0 ± 1.1 | 100.0 |
| Tropics | 7.04 ± 0.20 | 55 ± 3 | 41.3 ± 1.2 | 33.4 |
| Subtropics | 3.99 ± 0.25 | 31 ± 1 | 23.8 ± 1.5 | 32.9 |
| Extratropics | 1.75 ± 0.35 | 14 ± 2 | 10.2 ± 2.0 | 33.8 |
| Region | $P$ ($10^{14}$ kg day$^{-1}$) | $P$ (%) | $P$ (kg m$^{-2}$ day$^{-1}$) | $\tau$ (days) |
| Global | 15.1 ± 0.55 | 100 ± 0 | 2.96 ± 0.11 | 8.5 ± 0.5 |
| Tropics | 7.89 ± 0.55 | 52 ± 3 | 4.64 ± 0.32 | 8.9 ± 0.5 |
| Subtropics | 3.70 ± 0.46 | 24 ± 3 | 2.20 ± 0.28 | 10.9 ± 1.2 |
| Extratropics | 3.52 ± 0.31 | 23 ± 2 | 2.04 ± 0.18 | 5.0 ± 0.9 |

can be understood as the average time required to exchange the entire volume of the system. The turnover time is mathematically equivalent to the time constant of an exponential decay process (see section 1b). While in atmospheric hydrology the terms residence time, lifetime and turnover time have so far mostly been used interchangeably, a distinction as in other scientific disciplines (McGuire and McDonnell 2006) seems valuable, as shown below.

In catchment hydrology, the target quantity is sometimes not just an average age or time scale, but the full probability density function (PDF) of transit times of the outflow, the transit time distribution (McGuire and McDonnell 2006). In atmospheric hydrology, a corresponding age histogram, or *lifetime distribution* (LTD) have only recently become accessible (Winschall et al. 2014b; VT17; and this study). LTDs for the atmosphere obtained so far can be highly skewed and commonly have long, thin tails. For such distributions, it is known that central moments, such as the median or other percentiles may more reliably express the characteristics of the majority of precipitation water than a simple arithmetic mean. Ultimately, however, I argue that the full LTD should move into the focus of studies to characterize time scales in the atmospheric water cycle, and they are therefore a central topic of this study.

This study focuses on the tropospheric water, and in general excludes the stratospheric water cycle (and above) with its own particular transport mechanisms acting on the time scale of up to several years. It should, however, be noted that the 0.03% of stratospheric water vapor are part of the full LTD as well, and can serve as an illustrative example of the length of the thin tail of the LTD.

### b. The traditional approach

Traditionally, the atmospheric lifetime has been estimated from the turnover time. Calculating the turnover time of water vapor considers the (time averaged) atmosphere as a steady-state process with a single, well-mixed reservoir with a total water mass $W$ (e.g., Peixóto and Oort 1983; Trenberth 1998). The reservoir continuously loses mass by a precipitation flux $P$. Implicitly, the system will be constantly replenished by an equally large evaporation flux $E$ from the surface, and turns over its entire mass within $W/P$ days. The analogy to a steady-state lake system with rivers that provide continuous inflow and outflow ($E = P$) is evident. Alternatively, the time-mean properties of a nonsteady-state system can be obtained by long-term temporal averaging of the quantities. The evolution of the water mass in such a system can be described by an exponential decay process, where an initial mass $W_0$ at time $t = 0$ decreases by a decay constant $\lambda = P/W_0$ (e.g., Dettmann 2013):

$$W(t) = W_0 e^{-\lambda t}. \tag{1}$$

The turnover time in such a steady-state system is given by the decay time constant $\tau$, which in turn is obtained from the inverse of the decay constant $\lambda$ as $\tau = \lambda^{-1} = W_0/P$. Thereby, $\tau$ is the time it takes to deplete the water mass $W_0$ to $1/e$ of its initial mass, why it is sometimes also called an $e$-folding time, or turnover time. Following this approach, the turnover time can be obtained from measuring the outflow and size of the reservoir only, in other words, by considering its mass balance. Historically, this number has been calculated for the atmosphere directly from radiosonde data and surface precipitation measurements (Peixóto and Oort 1983). Using annual means of $W$ and $P$ from the 6-hourly ERA-Interim data, supplemented by 3-hourly forecasts for the year 2015 (Table 1), the decay time constant $\tau$ is

$$\tau = \frac{W}{P} = \frac{12.8 \times 10^3\ \text{km}^3}{551 \times 10^3\ \text{km}^3\ \text{yr}^{-1}} = 2.32 \times 10^{-2}\ \text{years} = 8.48\ \text{days}.$$

Unauthenticated | Downloaded 04/22/25 10:51 AM UTC

This result means a water reservoir in a stationary and homogeneous system (without "dead storage" of non-precipitating vapor) depletes to $1/e$ of its initial amount in 8.48 days, which is then identical to the mean age of water in the system (and the lifetime). Note that the exclusion of stratospheric water (0.03% of the total, or here 384 $km^3$), as done in this study, results in an identical result for the turnover time constant of $\tau = 8.48$ days. Including the stratospheric water with an assumed age of 1–2 years would increase the average age of all atmospheric water by about 0.2 days, whereas the turnover time (and the lifetime) would remain essentially unchanged. Such aspects are further explored in section 3.

According to recent estimates of these quantities from observations, the turnover time is 9.3 days (e.g., Trenberth 2011), almost 1 day longer than the estimate from reanalysis data obtained here. Similar findings apply to other reanalysis datasets. If the average lifetime can be calculated from a decay time constant, or turnover time, the larger value leads to the conclusion that the water cycle in ERA-Interim and other models is too intense and turns over too quickly. Evidently, the water cycle in ERA-Interim is affected by errors originating from the parameterization of subgrid-scale processes, as well as violations of mass conservation, due to analysis increments during the assimilation of humidity observations, for example, from radiosondes and satellites (Dee et al. 2011). Thus, one would expect deviations from the observed water cycle. At the same time, observations of the water cycle, in particular of precipitation and evaporation, are associated with substantial uncertainty as well (Trenberth 2011).

The present study is, however, not concerned with such differences between reanalyses and observations. The central question of this work is rather, how faithfully can a turnover time report the lifetime of tropospheric water vapor? How do heterogeneity and nonstationarity contribute to the LTD? And what are the findings and uncertainties of more advanced estimates regarding their capability to inform about the LTD? The ERA-Interim dataset, with a specific focus on selected years, hereby serves as an internally consistent test bed for investigating these questions pertaining to the atmospheric lifetime of water vapor.

### c. *Evaluation framework*

To investigate the ability of turnover time calculations to report water vapor age and lifetime for different systems, it is useful to recast the underlying exponential decay process [Eq. (1)] as a discrete sequence equation that is equivalent to the analytical expression. Hereby, the total atmospheric water content $W$ is reduced by a precipitation flux $pW$ while advancing by a time increment $\Delta t$ from time step $n$ to $n + 1$ [Eq. (2)]:

$$W^{n+1} = W^n - pW^n = (1-p)W^n = bW^n, \tag{2}$$

where $p$ and $b$ are related to the decay constant $\lambda$ as

$$b = 1 - p = e^{-\lambda \Delta t}. \tag{3}$$

Because of the approximate linearity of the $e$ function for small values, this expression can be approximated for small $\Delta t$ to obtain an intuitive view on the influences of both precipitation and evaporation on the lifetime in this framework. The simplified sequence equation contains the approximated precipitation flux $\lambda \Delta t W^n$ [Eq. (4)]:

$$W^{n+1} = W^n - \lambda \Delta t W^n = (1 - \lambda \Delta t) W^n. \tag{4}$$

Assuming implicitly that the precipitation flux is continuously replenished by an equivalent evaporation flux, the age of the moisture in the reservoir can now be calculated from Eq. (4). Over a time step $\Delta t$, a new water mass of age $\Delta t$ is added, and the remaining water mass in the reservoir ages by $\Delta t$. The average age of the total water mass is then obtained from a corresponding sequence equation for the age of moisture in the reservoir [Eq. (5)]:

$$A^{n+1} = (1 - \lambda \Delta t)(A^n + \Delta t) + (\lambda \Delta t)\Delta t, \tag{5}$$

with $A^n$ giving the atmospheric age of the reservoir water in dimensions of time at time level $n$. At each iteration (time step), a fraction $\lambda \Delta t$ of the reservoir is removed by precipitation, while the age of the remaining water fraction $(1 - \lambda \Delta t)$ increases by $\Delta t$ at each iteration. At the same time, evaporation contributes a fraction of new water $\lambda \Delta t$ with age $\Delta t$, replacing the loss through precipitation. The equation can be further simplified to

$$A^{n+1} = A^n(1 - \lambda \Delta t) + \Delta t. \tag{6}$$

The conceptual picture of water turnover in the atmosphere corresponding to this perspective involves an equal probability of removal from and recharge to all regions of the reservoir (Fig. 1a). In other words, the atmosphere is assumed to be well mixed, as indicated by the feathered arrows and circular arrow. In such a well-mixed system in steady state, the precipitation flux provides an unbiased sample of the age of the water vapor. Therefore, Eqs. (5) and (6) provide a single value for water vapor age and lifetime.

Using $W$ and $P$ provided by ERA-Interim for 2015, the average age given by Eq. (6) converges after about 60 iterations to a mean age of 8.5 days (Fig. 1b). Then the

Unauthenticated | Downloaded 04/22/25 10:51 AM UTC

turnover time is a faithful estimate of the mean age of the water vapor in the system, and identical with the lifetime. Figure 1b illustrates the advantage of considering an update equation such as given by Eq. (6), as it intuitively describes how the mean age of the atmospheric reservoir evolves in time. In the remainder of this manuscript, I will use and modify this general framework to obtain water vapor age and lifetimes for different variants of this system.

When obtaining and using a global mean value of the lifetime, one assumes two fundamental properties for the atmospheric water cycle:

1) Homogeneity: Water vapor is approximately well mixed throughout the atmosphere (or troposphere). There is therefore an equal probability of water vapor of all ages to contribute the precipitation flux with every rainfall event (Fig. 1a).
2) Stationarity: The reservoir mass and fluxes of water vapor, namely precipitation and evaporation, are in steady state. Therefore, average values of precipitation, evaporation, and water vapor mass characterize the time scale of the recharge and depletion process of the reservoir.

In catchment hydrology, nonstationarity and inhomogeneity are widespread and have prompted numerous complex study approaches (McGuire and McDonnell 2006). It is conceivable that these two conditions are also rarely fulfilled in the atmosphere. The few studies investigating the atmospheric LTD have shown a considerable spread in lifetimes between events and regions (Winschall et al. 2014b; VT17; and this study). The first aim of this study is to investigate now to what extent these properties are met in the atmosphere, and what role they play in shaping the LTD. I explore these aspects in the following using ERA-Interim data, and the framework introduced above.

## 2. Heterogeneity and nonstationarity of the atmospheric water cycle

To set the stage for the investigation of how the LTD is affected by heterogeneity and nonstationarity, I briefly recapitulate the spatial and temporal distribution of water vapor from vertical and horizontal snapshots.

### *a. Heterogeneity*

A global spatial mean of the vertical integral of water vapor from the bottom to the top of the ERA-Interim model atmosphere (at 0.1 hPa) at any given point in time shows that the troposphere (up to 200-hPa pressure, or a height of about 11 km above Earth's surface) contains about 99.97% of the atmospheric water (Fig. 2a; black line). By far most of the global water vapor is located at even lower layers. The integrated fraction of column water reaches 96.1% below 500 hPa (about 5.5 km), the lower half of the atmosphere's mass, and 80% reside within the lowermost 25% of the atmospheric mass (below 750 hPa; Fig. 2a; gray line). The logarithmic shape is a result of the interplay of thermodynamic and dynamic factors, such as the decreasing saturation vapor pressure with decreasing temperature, and mixing between evaporation sources at the surface and drier air aloft in different stability conditions (Held and Soden 2006). Homogeneous (well mixed) conditions would imply that the moisture in the atmosphere up to 11 km is turned over entirely within 8–10 days. The fact that the troposphere is indeed not well mixed with respect to water vapor is underlined by the large difference between the integrated fractions of water vapor and of atmospheric mass (Fig. 2a; black and gray lines).

What appears as a continuous profile of water throughout troposphere on a global average is often a heterogeneous combination of layers of different stability when considered locally and instantaneously. Randomly selected humidity profiles at individual grid points (Fig. 2a, blue lines) at 0000 UTC 19 December 2006 vary strongly between the tropics (0°, 0°; dotted), subtropics (20°S, 0°; solid) and extratropics (50°N, 0°; dashed). The subtropical profile shows a typical case for these latitudes, with most water vapor contained below the trade inversion at 900 hPa, and topped by an almost dry atmosphere above dominated by subsidence. One can expect that such differences imply quite different transport pathways and thus water vapor lifetimes in boundary layer and free-troposphere air in these regions.

Average $W$ for the three regions, expressed here as the global average integrated water vapor (IWV), varies little for the tropics (41.3 kg m$^{-2}$) and subtropics (23.8 kg m$^{-2}$), more so for the extratropics (10.2 kg m$^{-2}$; Table 1). Instantaneous pictures of vertically IWV show substantial spatial heterogeneity (Fig. 2). The horizontal distribution of IWV at any arbitrary date (again here 0000 UTC 19 December 2006) shows the tropics (between 20°S and 20°N) standing out as a belt where IWV generally exceeds 30 kg m$^{-2}$ (Fig. 2b; green to red shading), with some zonal variation to much higher values, related to the time of day and the land–ocean distribution. The subtropics (defined here between 20° and 50°S and between 20°–50°N, respectively) show substantial variation between low and high values of IWV (4–50 kg m$^{-2}$). The extratropics and polar regions (defined here north and south of 50°N and 50°S, respectively) are dominated by values below 20 kg m$^{-2}$, with local excursions of higher values related to extratropical frontal systems (Fig. 2b; blue shading). The sharp

Unauthenticated | Downloaded 04/22/25 10:51 AM UTC

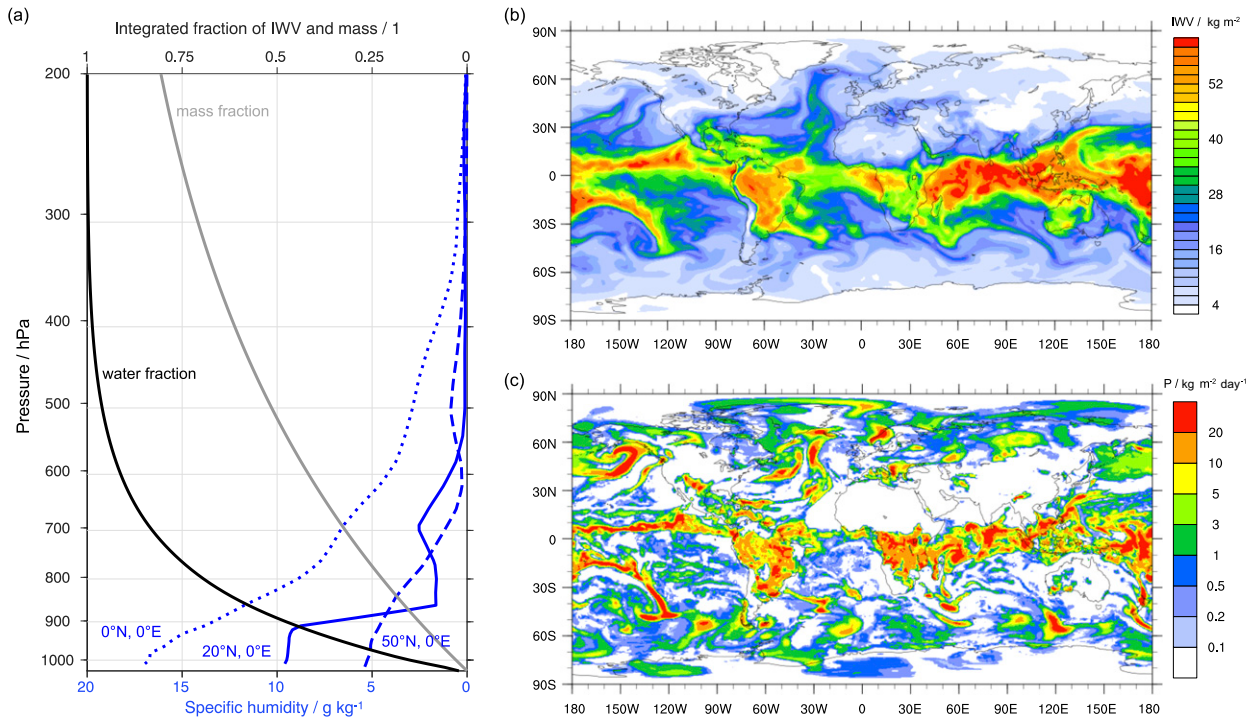


FIG. 2. Examples for inhomogeneity in the water cycle obtained from ERA-Interim data for 0000 UTC 19 Dec 2006. (a) Vertical profiles of specific humidity at latitudes 0°, 30°, and 60°N (blue lines). Black line shows the global average of the fraction of vertically integrated water vapor (IWV) for the pressure-level ranges from 1000 to 200 hPa. (b) IWV (kg m$^{-2}$) and (c) 6-h precipitation (kg m$^{-2}$ day$^{-1}$) at 0000 UTC 19 Dec 2006.

gradients associated with such excursions are washed out to a broad gradient in a monthly average view or longer-time climatological mean (e.g., Gimeno et al. 2012), but are relevant for the local LTD.

Day-to-day variations of $P$ in the three regions are substantially larger than for IWV, and partly compensate in the global mean (Table 1). The subtropics and extratropics show a similar and much lower areal average precipitation rate (2.20 and 2.04 kg m$^{-2}$ day$^{-1}$) than the tropics (4.64 kg m$^{-2}$ day$^{-1}$). Large areas are devoid of precipitation at any instance at all latitudes, while others show a wide range of precipitation rates (Fig. 2c). The 3-h precipitation total can reach a similar amount in extratropical and tropical regions (above 10 kg m$^{-2}$ day$^{-1}$), albeit with lower overall areal coverage (Fig. 2c; orange to red shading). The ratio of $W$ and $P$, which determines the turnover time, varies both meridionally and zonally when considered locally and at a particular time instance. Average turnover times $\tau$ [Eq. (1)] for the three zonal sectors are therefore different, and show substantial day-to-day variability (Table 1; section 3).

### b. *Nonstationarity*

Next, I recapitulate how nonstationarity is manifested in the atmospheric water cycle. In the calculation of the areal average precipitation rates above, it was assumed that all of the region's surface area participates equally in the water cycle. At any given time instance, this is, without surprise, not the case (Fig. 2c).

Analyzing the frequency of precipitation over an area for longer time periods, one can obtain a more general insight into the stationarity of precipitation. Figure 3a shows the probability that the daily precipitation rate exceeds 1 kg m$^{-2}$ day$^{-1}$ at any grid point of the ERA-Interim data during 2015. The narrow tropical rain belt stands out as an area where the daily precipitation total exceeds 1 kg m$^{-2}$ day$^{-1}$ on more than 80% of days. The extratropics in contrast have only a 30%–40% probability to exceed this daily precipitation threshold, mostly along the storm tracks. The subtropics in between stand out as large regions with an overall small, but nonzero probability to experience such daily precipitation rates. These findings from ERA-Interim data indicate that local deviations from a global daily average precipitation rate of 2.96 kg m$^{-2}$ day$^{-1}$ are generally large. In fact, in a cumulative distribution of annual mean precipitation, 50% of the global precipitation fall on less than 25% of the surface area, while 90% of the global precipitation fall on about two-thirds of the surface

Unauthenticated | Downloaded 04/22/25 10:51 AM UTC

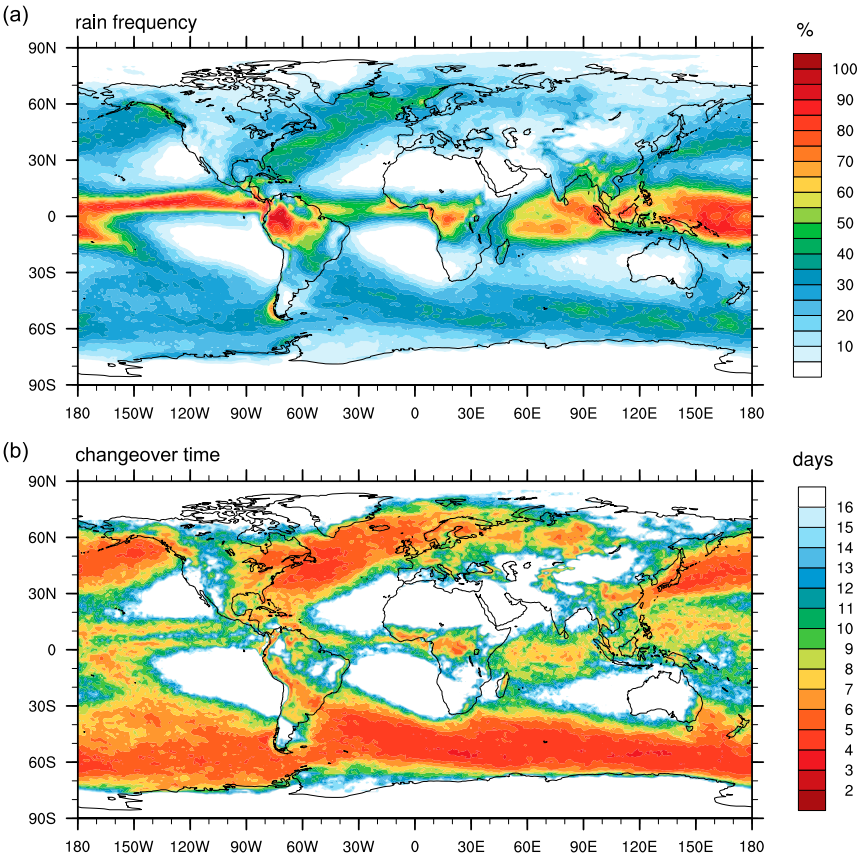


FIG. 3. (a) Probability for daily precipitation to be larger than 1 kg m$^{-2}$ day$^{-1}$ (shading; %). (b) Changeover time (days) between either a series of precipitation days ($p > 1$ kg m$^{-2}$ day$^{-1}$) or break days ($p \leq 1$ kg m$^{-2}$ day$^{-1}$). Both panels were obtained from 3-hourly ERA-Interim data for the year 2015.

(not shown). As could be expected, nonstationarity of precipitation appears as the rule rather than the exception, with potential consequences for the local LTD.

A more targeted measure of the intermittency of precipitation is the *changeover time* $t_c$. This measure is calculated by counting the average number of times that a precipitation period (daily total $P > 1\,\mathrm{kg\,m^{-2}\,day^{-1}}$) is interspersed by break periods ($P \leq 1\,\mathrm{kg\,m^{-2}\,day^{-1}}$) at each grid point in the ERA-Interim data. Dividing the number of days analyzed (here 365 days for the year 2015) by the number of break periods then provides the average changeover time $t_c$ in units of days (Fig. 3b). Large regions in the extratropics stand out with a $t_c$ of 3–6 days (red shading), indicating a high intermittency of precipitation. In the subtropics, the Arctic and some continental regions where precipitation falls less frequently at these rates, the change from break to rain or back occurs on average after more than 16 days (Fig. 3b, white shading). Tropical regions have intermediate changeover times, indicating a more stationary regime, but with precipitation as the normal state. Here, a $t_c$ of 6–10 days is most common (Fig. 3b, orange and green shading). While the $t_c$ may be influenced by known deficiencies in reanalysis-based precipitation fields (Trenberth 2011), the qualitative results are only weakly sensitive to the precipitation threshold.

In summary, a sizable portion of Earth's surface, in the subtropics and high latitudes, receives precipitation quite rarely. However, when it precipitates in subtropical dry areas, for example, precipitation rates are typically much larger than suggested by the annual average (cf. Fig. 2b). Many regions of the world receive moderate to intense rainfall on short time scales from different weather systems, interspersed by dry periods of different duration. Horizontal and vertical heterogeneity and nonstationarity will be evident in the atmospheric water cycle at any random instant in the ERA-Interim dataset. Therefore, one can argue that a system divided into different compartments, or subwater cycles, may be a more realistic representation of

Unauthenticated | Downloaded 04/22/25 10:51 AM UTC

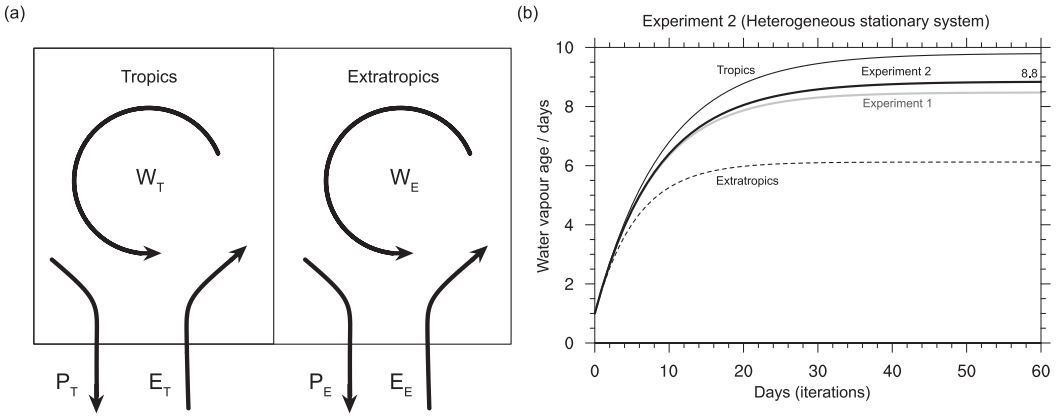


FIG. 4. Water vapor age calculation for a heterogeneous, stationary system. (a) Illustration of the budget of the atmospheric water content of (left) a tropical reservoir $W_T$ and (right) an extratropical reservoir $W_E$, each well mixed and with its own flux components for evaporation ($E_T$, $E_E$) and precipitation ($P_T$, $P_E$). (b) Evolution of the water vapor age for the heterogeneous, stationary system (Experiment 2) and the two compartments, tropics (thin solid) and extratropics (dashed), obtained using Eq. (7). The global mean age stabilizes at 8.8 days after about 50 iterations. Result from Experiment 1 shown as reference (gray line).

the atmospheric water cycle. I now investigate meridional differences in turnover time using the framework proposed above, in idealized heterogeneous and nonstationary systems.

## 3. Turnover time in a heterogeneous water cycle

A turnover time can now be calculated separately for each of the compartments, or regions, defined above. Dividing the atmosphere into these compartments, where each represents about equal shares of Earth's surface (Table 1), yields that on an annual average of the study period in 2015, about 55% of the global water mass $W$ are in the tropics, 31% in the subtropics, and 14% in the extratropics. For precipitation mass $P$, the shares amount to approximately 52%, 24%, and 23%, respectively (Table 1).

The ratio of $W$ over $P$ ($\tau$) also indicates substantial differences between these compartments. Using Eq. (5) or Eq. (6), the corresponding turnover time constants become 8.9 days for the tropics, 10.9 days for the subtropics, and 5.0 days for the extratropics (Table 1). The difference in $\tau$ could be interpreted as a different intensity of the atmospheric water cycle in the three compartments. Here, the larger relative precipitation flux in the extratropics results in a more-than-2-times-faster turnover time compared to both other compartments.

The short turnover time in the extratropics may be affected by an unknown fraction of the water vapor originating from evaporation farther south, and being transported poleward within atmospheric rivers and tropical moisture exports (Knippertz and Wernli 2010; Sodemann and Stohl 2013). The 5-day turnover time is, however, close to the extratropical values obtained by LS16 (4.0 days), and the recent study by (Papritz and Sodemann 2018) finds lifetimes (precipitation age based on water vapor tracers) as short as 1–2 days during Arctic cold-air outbreaks. A substantial part of the tropical precipitation may have evaporated in the subtropics and traveled some distance before precipitating in the intertropical convergence zone (ITCZ). These examples point to heterogeneity as a potential factor in creating observed LTDs. While the separation into several meridional compartments that each are internally homogeneous (well mixed), is a coarse simplification of the atmospheric water cycle, the results obtained here also underline the limited use of one global average value for the turnover time when estimating the lifetime in a specific region or location (LS16, see section 5).

A reservoir mass-weighted average of the three time constants obtained for the three compartments results in a global average water vapor age of 9.0 days, about 0.5 days longer than the 8.5 days obtained for the global system. The turnover time, calculated from a weighted average of the fluxes, however, remains unchanged at 8.5 days. Thus, by partitioning the system into subsystems, the total average age increases, while the turnover and therefore the approximated mean lifetime remain unchanged. Next, I investigate this behavior more systematically in a simplified two-compartment system.

### *Generalized heterogeneous system*

Consider now a partitioning of the atmospheric water mass into the two compartments, tropics (subscript $T$)

Unauthenticated | Downloaded 04/22/25 10:51 AM UTC

TABLE 2. Characteristics of the water cycle obtained from daily ERA-Interim data for the year 2015. Values are provided for the global average and for zonal averages for two regions—tropics and extratropics—that divide Earth's surface area into equal halves, with daily standard deviations.

| Region | $W$ ($10^{15}$ kg) | $W$ (%) | IWV (kg m$^{-2}$) | Area (%) |
|---|---|---|---|---|
| Global | 12.8 ± 0.57 | 100 ± 0 | 25.0 ± 1.1 | 100.0 |
| Tropics | 9.43 ± 0.19 | 74 ± 3 | 36.4 ± 0.7 | 50.0 |
| Extratropics | 3.34 ± 0.49 | 26 ± 2 | 13.3 ± 2.0 | 50.0 |
| Region | $P$ ($10^{14}$ kg day$^{-1}$) | $P$ (%) | $P$ (kg m$^{-2}$ day$^{-1}$) | $\tau$ (days) |
| Global | 1.51 ± 0.05 | 100 ± 0 | 2.96 ± 0.11 | 8.8 ± 0.5 |
| Tropics | 0.96 ± 0.05 | 64 ± 2 | 3.71 ± 0.17 | 9.8 ± 0.5 |
| Extratropics | 0.55 ± 0.04 | 36 ± 2 | 2.18 ± 0.17 | 6.1 ± 0.8 |

and extratropics (subscript $E$), as illustrated in Fig. 4a. Each compartment represents 50% of Earth's surface area. Assuming that these two compartments each have their own water cycles, one can calculate the global mean lifetime $\overline{\tau}$ by first considering each separately and then calculating a mass-weighted average. Here, the tropical water mass fraction $m$ of the total mass $W = W_T + W_E$ is given by

$$m = W_T/W,$$

and the tropical precipitation flux ratio $f$ of the total precipitation $P = P_T + P_E$ is

$$f = P_T/P.$$

The fractions for the extratropical counterparts can be written as

$$1 - m = W_E/W = (W - W_T)/W \quad \text{and}$$
$$1 - f = P_E/P = (P - P_T)/P.$$

The weighted mean turnover time $\overline{\tau}$ becomes

$$\overline{\tau} = f\left(\frac{mW}{fP}\right) + (1-f)\left[\frac{(1-m)W}{(1-f)P}\right], \qquad (7)$$

with $W$ in kg and $P$ in kg m$^{-2}$ day$^{-1}$. With the numbers in Table 2 and using Eq. (6), one obtains a moisture age and turnover time for the tropics $\tau_T = 9.8$ days, and an extratropical $\tau_E = 6.1$ days (Fig. 4b). Since the turnover time is a property of the fluxes rather than the reservoir mass, the average turnover time $\overline{\tau}$ becomes identical to the homogeneous system (8.5 days) when weighting by the fractions of global precipitation flux.

Similarly, the weighted mean water vapor age can be obtained from a weighted average of the turnover times by using the mass fractions as weight. The mass-weighted water vapor age of the heterogeneous system is then $\overline{\tau} = 8.8$ days, again higher than the globally homogeneous value (8.5 days), but lower than the age of the three-compartment system (8.9 days). Stepping through the entire set of combinations of flux and compartment size ratios from Eq. (7) results in a surface with minimum average ages along the diagonal (Fig. 5a). A specific example for the reservoir ratio $m = 0.75$ and flux ratio $f = 0.10$ to 0.90 provides a total average age ranging from 30 to 12 days, with a minimum at 8.5 days at a flux ratio of 74% (Fig. 5b; black line). Picking another example with $m = 0.50$ shows a similar general pattern, with a total average age of 18 days on both ends, and a minimum of 8.5 at $f = 50\%$ (Fig. 5b; gray line). These two specific examples, and the general picture for all cases (Fig. 5a) show that minimum ages in this system are found if the flux ratio and reservoir ratio are equal, or in other words, if the system is homogeneous. In all other cases, the mean age becomes larger.

It appears that in the vertical additional components could be added in this idealized representation of the water cycle. Again, the average age would increase, whereas the mean turnover remains unaffected by heterogeneity. The fact that the turnover time is then no longer an unbiased sample of the reservoir age is a key prerequisite for understanding the existence of long tails in the LTD, that enters precipitation as a small contribution from long-lived vapor. Given the both horizontal and vertically abundant heterogeneity of the atmospheric water cycle, turnover times appear limited in their ability to reliably estimate the range of lifetimes occurring within the LTD. I now continue by investigating the effect of nonstationarity on the LTD.

## 4. Turnover time in a nonstationary, homogeneous water cycle

Contrary to the stationary system (Fig. 1a), the fluxes $E$ and $P$, and therefore also $W$, are not constant in time in a nonstationary system. For example, precipitation may be zero for 3 days in sequence, while on day 4 there is 4 times the daily precipitation as in the stationary

Unauthenticated | Downloaded 04/22/25 10:51 AM UTC

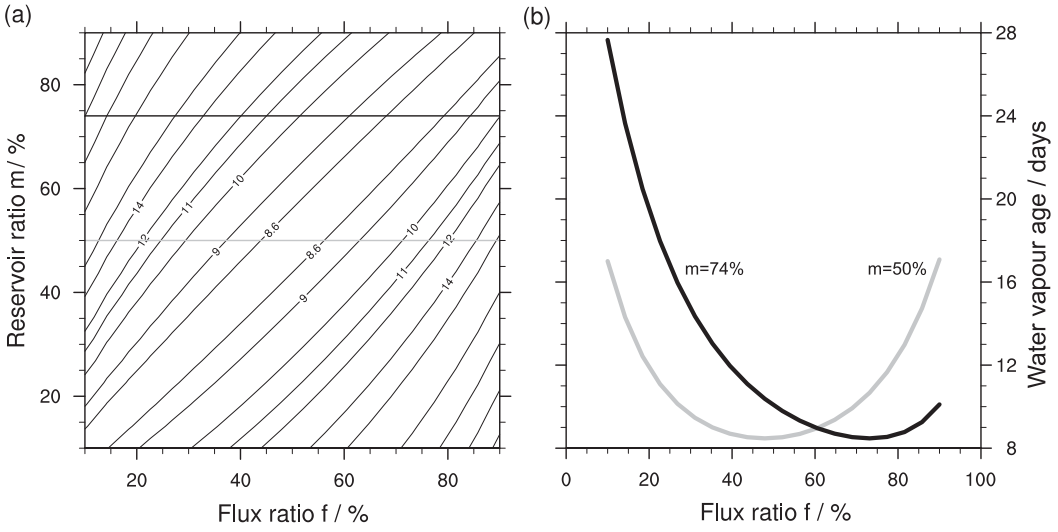


FIG. 5. (a) Dependency of the average water vapor age (contours; days) for a two-compartment system on the reservoir ratio $m$ and flux ratio $f$. (b) Dependency of the water vapor age on the flux ratio for a reservoir ratio of $m$ = 74% (black) and $f$ = 50% (gray), as indicated by the horizontal lines in (a).

case (Fig. 6a). Mass balance will thereby be maintained by the larger rainfall on day 4. At a 4-day average, therefore, the fluxes in the nonstationary system will be the same as in the homogeneous case (Fig. 1). In the examples considered here, $P$ will be allowed to vary in time, while $E$ is kept constant for simplicity. The resulting variation of the total water mass $W$ with time will allow for lower ages than in the stationary system, while the temporal average of $W$, and therefore the turnover time, remain unchanged.

For the nonstationary, homogeneous system the sequence equation changes compared to the stationary case [Eq. (4)] due to the time variation of the fluxes. In the budget equation

$$W^{n+1} = W^n - P^n \Delta t + E^n \Delta t, \tag{8}$$

$W^n$ and $W^{n+1}$ are the time-varying mass of the water reservoir, and $P^n$ and $E^n$ are the time-varying fluxes. For example, setting $P^n \in [0, 0, 0, 4\overline{P}]\,\mathrm{kg\,m^{-2}\,day^{-1}}$ (see Fig. 6a) forms a sequence of days with and without precipitation. Averaged over the number of days of a sequence, the quantities will equal their long-term means ($\overline{W}$, $\overline{E}$, and $\overline{P}$).

The water vapor age is accordingly calculated from the sequential calculation of an update equation where the new age is obtained from the increased age of the remaining water mass, and the age of the newly added water mass, divided by the new total:

$$A^{n+1} = \frac{(W^n - P^n \Delta t)(A^n + \Delta t) + E^n \Delta t}{W^n - P^n \Delta t + E^n \Delta t}. \tag{9}$$

Considering precipitation as an nonstationary process, and evaporation as a continuous one, the following example can be calculated: $E$ is constant at a value of $15.1 \times 10^{14}\,\mathrm{kg\,m^{-2}\,day^{-1}}$, and $P$ is zero for 3 days, then $4 \times 15.1 \times 10^{14}\,\mathrm{kg\,m^{-2}\,day^{-1}}$ on the fourth day. Here, $W$ evolves in time, with an initial value of $10.62 \times 10^{15}$ kg. This combination yields an average, but time-varying water vapor age of 8.35 days (Fig. 6b; stippled line), about 0.13 days less than the homogeneous system. This can be understood such that as $W$ varies in time (Fig. 6c), the evaporation process can more efficiently ''rejuvenate'' the atmospheric water on day 4, leading to overall lower ages.

This behavior can be illustrated returning to the analogy of a lake system with an inflow and outflow. When a large amount of freshwater leaves the lake in a short time, the lake level is lowered, and incoming water will lead to a lower average age of the lake water than if a larger water volume were in the reservoir.

Thus, when conditions deviate from stationarity, it is possible to obtain lower mean water vapor ages than expected from the turnover time for a homogeneous system, or than calculated from a long-term average. Two more pronounced examples further illustrate the point that nonstationary conditions can lead to shorter water vapor ages. For a nonstationary precipitation process with intense precipitation every eighth and twelfth day (Fig. 6b), the average age decreases to 7.74 and even 7.03 days (Fig. 6b; thick and thin solid line). While starting at different values, $W$ remains at $12.8 \times 10^{15}$ kg on average (Fig. 6c). The turnover time for this system is notably unchanged,

Unauthenticated | Downloaded 04/22/25 10:51 AM UTC

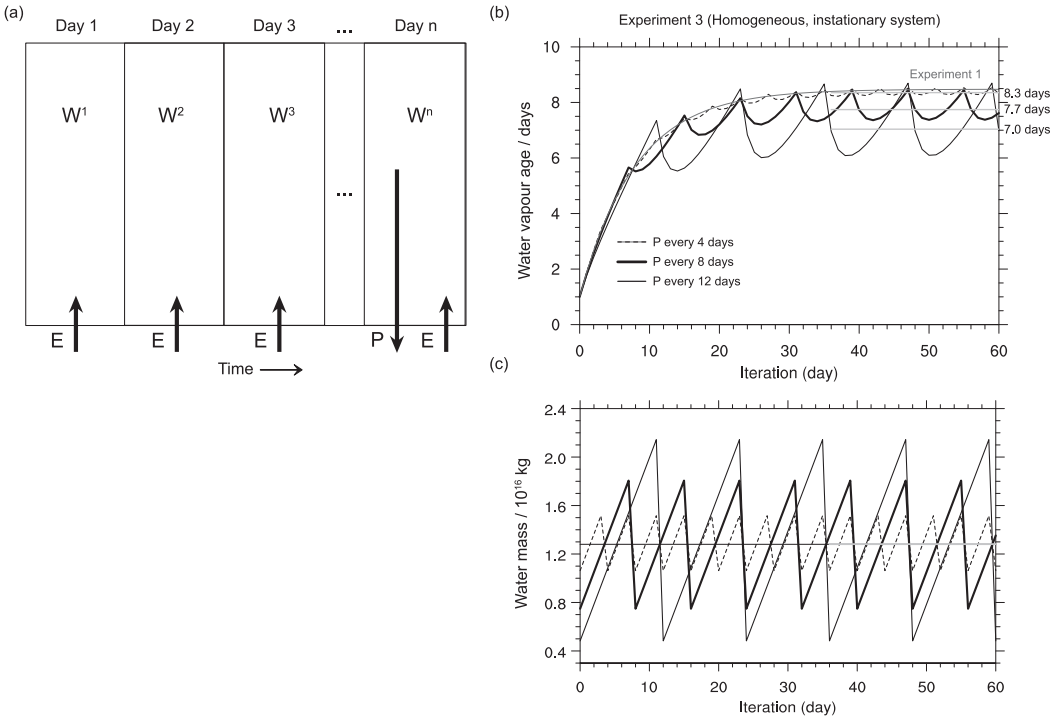


FIG. 6. Water vapor age calculation for a homogeneous, nonstationary system. (a) Illustration of the temporal evolution budget of the atmospheric water content $W^n$ at each day $n$. Evaporation flux $E$ is constant every day, while precipitation $P$ is zero on days 1 to $n-1$ and occurs on day $n$ with $P = nE$. (b),(c) Evolution of the water vapor age and water mass, respectively, for the homogeneous, nonstationary system (Experiment 3) using Eq. (9) and 4, 8, and 12 days between precipitation events. After about 60 iterations, the 20-day average water vapor age stabilizes at 7.8, 7.2, and 6.1 days, respectively. Precipitation occurs at peak water vapor age.

as $\overline{W}$ and $\overline{P} = 15.1 \times 10^{15}\,\mathrm{kg\,m^{-2}\,day^{-1}}$ (Fig. 6c) result in $\tau = 8.48$ days.

Considering the lifetime of the water vapor, that is, the precipitation age, it can be seen that precipitation first occurs at the time when the water vapor has reached the maximum age of the sequence of about 8.5 days, as imposed by the constraint of a constant $W$ over time (Fig. 6c). As in the experiment with nonhomogeneous atmospheric compartments (section 3), the water vapor lifetime is no longer a predictor of the water vapor age, but remains consistent with the turnover time.

While the example given here is artificial in that it includes the entire atmosphere, precipitation processes can substantially deplete the total column water locally within a short time. One example are cases where the water vapor contained in an atmospheric river impinges on a topographic rise, leading to localized, intense condensation and precipitation with drier air masses downstream (e.g., Ralph et al. 2011; Sodemann and Stohl 2013). Eventually, evaporation downstream will produce regions of ''young'' water vapor, and precipitation from this vapor in turn can be younger than suggested by a global stationary system. It is conceivable that similar processes are at play in all weather systems where precipitation forms, including tropical deep convection, midlatitude storms, and orographic precipitation, among others.

Concerning the LTD, including nonstationarity explains how short-lived water vapor can originate, and become part of the full lifetime distribution. However, the age of the remaining water will increase accordingly, and its participation in precipitation processes will eventually create relatively older precipitation. Including nonstationarity to the evaporation flux will allow countless other combinations of fluxes, that are not explored further here. In combination with heterogeneous conditions, an LTD can be expected where a shift of part of the lifetimes to younger age will cause a corresponding contribution on the longer end of the tail, thereby potentially creating a wide range of values in real atmospheric weather systems. This concept provides a key perspective for understanding the discrepancies between the short water vapor lifetimes found by the LS16 and the mean value expect from mass balance considerations:

If the majority of the lower-level humidity is depleted and replenished frequently, as one could expect from the proximity of most water vapor to the surface, it would obtain a relatively young age, in line with the time

Unauthenticated | Downloaded 04/22/25 10:51 AM UTC

scale of weather systems that deplete and replenish the atmosphere. At the same time, the considerably smaller fraction of water vapor in the layers above will be relatively older, depending on its transport process for example within the Hadley circulation, or ascending in warm conveyor belts and returning by subsidence in anticyclones on the order of weeks. As long as the water vapor participates in the precipitation process at some point, this water vapor will contribute small amounts with a large age, that are then removed from the atmosphere at layers where precipitation is more active, thus keeping the mean lifetime near the about 8.5 days expected from the turnover time. A small amount of slowly overturned water vapor would thus constantly ''seep'' back into the precipitation cycle, for example when dehydrated air masses descending from the middle and upper troposphere return toward the surface and participate in the evaporation process. As is discussed below, the method of LS16 possibly underestimates such mixing processes, and could miss such small contributions from long-lived water vapor to precipitation. The LS16 method would thus report lifetimes closer to the median of the LTD, ignoring the long, thin tail.

At this point, I conclude that turnover times capture only a single aspect of the LTD in the case of nonhomogeneous and nonstationary systems, which is not necessarily useful for many applications of the lifetime. Other approaches are needed to reliably characterize the heavily skewed LTD, and that are representative for the majority of the precipitation. While one thereby would like to take into account the spatial and time-varying complexity of atmospheric processes affecting water vapor as comprehensively as possible, I first seek to obtain some guidance on how far the majority of water vapor is expected to travel based on a simple and independent Eulerian plausibility check.

## 5. A plausibility check using the vapor transport speed

A simple plausibility check of an expected lifetime can be conducted by considering the transport distance $\Delta_\eta$ that water would travel on average for a given lifetime. This information is accessible by considering the product of a lifetime $\eta$ and a vertically and time-averaged vapor transport speed $\mathbf{v}_v$:

$$\Delta_\eta = \mathbf{v}_v \eta. \tag{10}$$

Hereby, the vertically averaged vapor transport speed $\mathbf{v}_v$ at each column is calculated as

$$\mathbf{v}_v = \frac{1}{g\mathrm{IWV}} \int_{p_0}^{p_t} q\mathbf{v}\, dp. \tag{11}$$

This humidity-weighted wind velocity is a straightforward Eulerian diagnostic that provides the mean horizontal speed of water vapor at any given grid point. As many regions have a prevailing wind direction, $\mathbf{v}_v$ can be used to estimate an expected transport distance $\Delta_\eta$ for a given lifetime $\eta$.

The average transport distance for the month of January 2015 in the ERA-Interim dataset shows pronounced maxima of 15–20 $\mathrm{m\,s^{-1}}$ in the extratropics, and lower values of about 3–8 $\mathrm{m\,s^{-1}}$ in the tropics (Fig. 7; shading). The patterns of moisture transport speed are coincident with the lower-tropospheric wind pattern of the storm tracks, where both specific humidity and wind speed are high (not shown).

When applying the 8.5-day lifetime obtained for the homogeneous system above, and as found by VT17 for the extratropics, one obtains transport distances $\Delta_\eta$ of ~12 800 km in the extratropics (considering a transport speed $\mathbf{v}_v \approx 17.5\,\mathrm{m\,s^{-1}}$). A precipitation event in the extratropics (e.g., at 50°N, 0°) would then on average receive its moisture from regions beyond the U.S. West Coast, far into the Pacific (Fig. 7; black dashed contour). This seems at odds with the observation that strong heat fluxes moisten dry continental air as it moves over warm sea surface temperatures in the North Atlantic during wintertime (e.g., Cayan 1992; Persson et al. 2005; Papritz et al. 2014). When using a lifetime of 4.5 days or less, that according to published atmospheric LTD studies would be more representative of the majority of the precipitation, most of the moisture would remain within a distance of ~6800 km, with the North Atlantic as the mean moisture source (white dashed contour).

Using again a global average turnover time of 8.5 days, moisture precipitating in the tropics (Brazil; 0°, 50°W) would on average travel $\Delta_\eta = 4000$ km with $\mathbf{v}_v \approx 5.5\,\mathrm{m\,s^{-1}}$, locating sources at 30°N (black solid contour). Results from VT17 show an even longer local lifetime average of 10–11 days in that region. While the advection may not be along a direct path, these sources are relatively far away to be representative of the majority of the moisture, as strong evaporation occurs at latitudes south of 30°N. Using a lifetime of 4.5 days, an average transport range of ~2100 km results for the tropics. Water would thus be sourced in the more immediate regions of the ITCZ of up to 20°N (or 20°S), tapping into the strong evaporation regions in the subtropics (Fig. 7, white contours).

According to this simple measure, a lifetime of 8.5 days appears less plausible than 4.5 days, in particular for the extratropics. Since water vapor with long lifetimes can clearly exist in the atmosphere, the

Unauthenticated | Downloaded 04/22/25 10:51 AM UTC

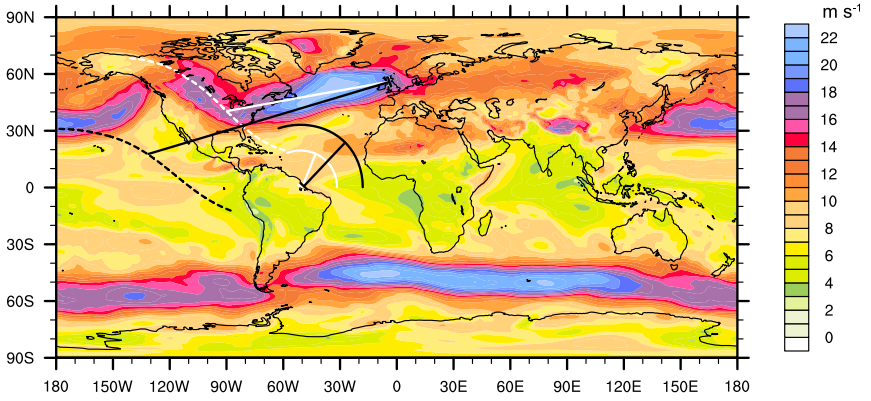


FIG. 7. Humidity-weighted vertical average wind speed (shading; m $s^{-1}$) during Jan 2015, calculated from 6-hourly ERA-Interim data. The map can be interpreted as a proxy for the horizontal transport speed of water vapor in the atmosphere. Solid and dashed arcs show horizons of horizontal moisture transport distance in the approximate mean wind direction for an extratropical location (55°N, 0°; stippled lines) and a tropical location (0°, 50°W; solid lines) calculated with lifetimes of 4.5 (white lines) and 8.5 days (black lines). See text for details.

average lifetime, as obtained by the turnover time, is strongly affected by a heavily skewed LTD. As a result, the average lifetime does not provide representative guidance for where the majority of the precipitation water would originate. Instead, a value close to the median, or some other percentile, may prove as more informative. In the following section, I provide an updated analysis and interpretation of the results of LS16, before discussing several existing methods, and indicating a potential way forward in estimating the LTD.

## 6. An update to the results of LS16

The results by LS16 yielded global maps of lifetimes consistent with weather system patterns, with an average of 3.9 days globally, and an upper estimate of 4.4 days due to unaccounted moisture. In their manuscript, LS16 reported only results for the lifetime of water vapor that were mixed into air parcels within the boundary layer. However, almost 50% of the global moisture enter air parcels within the free troposphere, mostly thought to be related to moist convection that blends boundary layer moisture into air parcels in the free troposphere (Winschall et al. 2014a). Here I provide an update to the results of LS16 for the entire troposphere, and reinterpret the obtained lifetimes in light of the findings above as median values of the LTD, rather than mean values. The method itself is briefly discussed in section 7.

The analysis of LS16 was repeated for the year 1993 as a representative example period. When including free-tropospheric moisture uptakes, the mean lifetime increases from 3.90 days by about 1 day to a global annual average of 4.81 days (Fig. 8a). The spatial patterns remain thereby very similar to the results in LS16. A zonal mean of the lifetime shows increases of up to 0.5 days in parts of the subtropics and tropics (Fig. 8b; black dashed and solid lines). Comparison of the area and precipitation weighted probability density function of the local lifetime for all precipitation events in the 1-yr period shows that the mean shifts by about 0.5 days for the analysis including the entire atmosphere, in particular due to a thicker right tail (Fig. 8d). As is discussed in section 7, the WaterSip method likely misses mixing events where relatively old water vapor enters back into the precipitation cycle. The method is designed to identify substantial increases of the specific humidity, such that mixing processes with equally dry or drier air will remain undetected. When interpreted as the mean lifetime of the full LTD (VT17), this characteristic causes a discrepancy to expectations. However, when considering the typical shape of LTDs, the WaterSip method will pick up substantial moistening events, but miss out on mixing with drier air that contains older water vapor constituting the tail of the LTD. The average lifetimes reported by the WaterSip method can therefore be interpreted as a value close to the median of the full LTD. Note that with a contribution of about 10%–15% of long-lived vapor of 20 days or more (rather than the 5% estimated by LS16), the mean lifetime would come close to the estimate from methods using a well-mixed assumption. When aiming at robust and interpretable results about the turnover of the majority of the water vapor in the climate system,

Unauthenticated | Downloaded 04/22/25 10:51 AM UTC

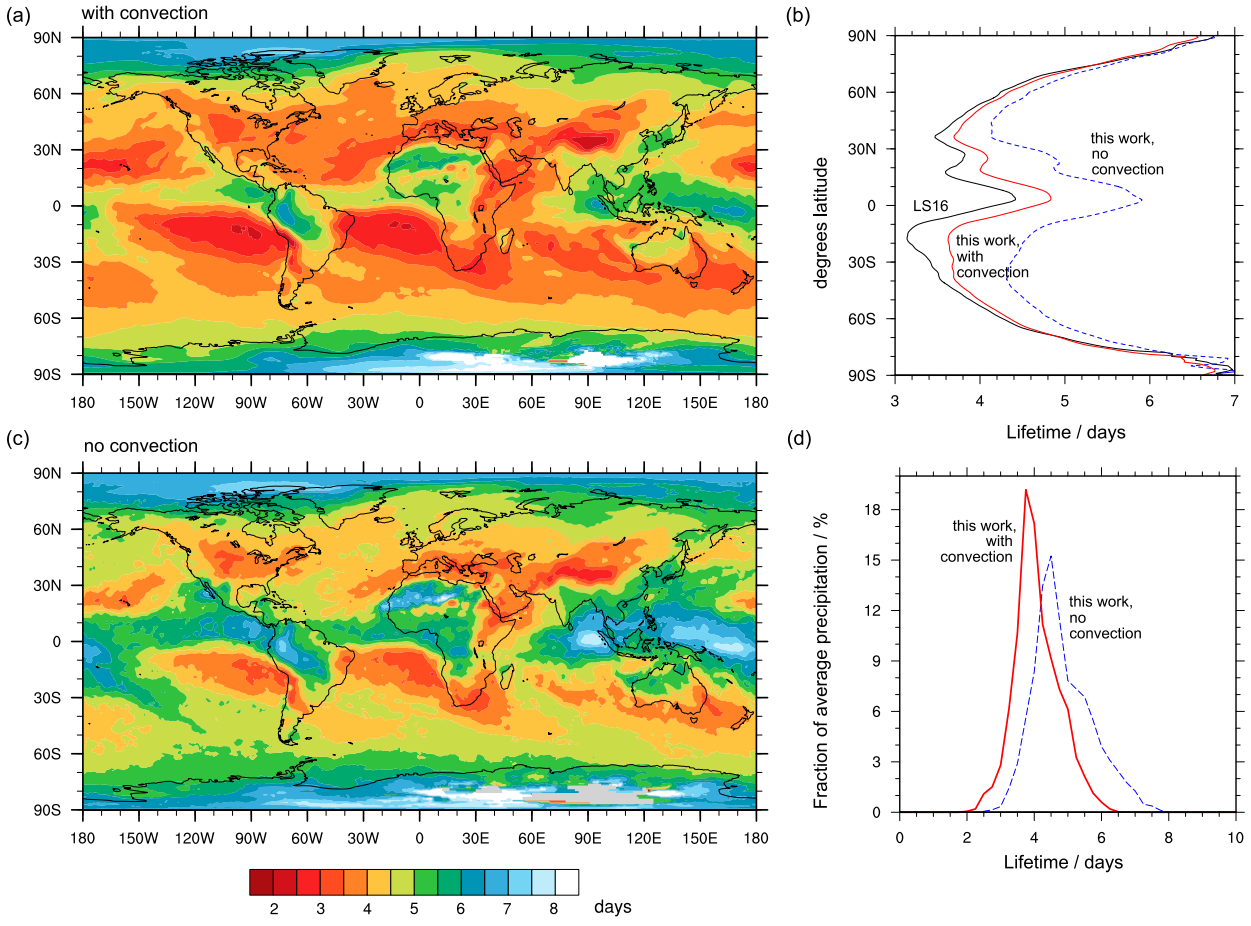


FIG. 8. Sensitivity analysis of lifetimes from the Lagrangian diagnostic for the year 1993 based on FLEXPART calculations with ERA-Interim data. (a) Annual mean lifetime (days) for a trajectory dataset with the FLEXPART convection parameterization enabled. (b) Zonal means of the lifetime from LS16 (black line) and results from the present study with convection enabled [as shown in (a); red line], and with convection disabled (blue dashed line). (c) As in (a), but with convection parameterization disabled in the underlying FLEXPART model simulation. (d) Spatial probability density function of precipitation-weighted annual mean lifetimes with convection enabled (red line) and disabled (blue dashed line).

I argue that such a small fraction of the water vapor should not be a decisive element.

*Sensitivity experiment*

To obtain a measure of the uncertainty of the LS16 results for the median lifetime, the Flexible Particle dispersion model (FLEXPART) and subsequent WaterSip analysis was repeated for the year 1993 without convection parameterization. Turning off the convection scheme degrades the trajectory simulation due to an underestimation of vertical transport. The sensitivity simulation can, however, serve as an upper bound on the uncertainty from additional interpolation errors due to inconsistencies between the ERA-Interim and FLEXPART convection schemes. Results of the approximated medium lifetime for the sensitivity simulation (Fig. 8c) show still the same patterns. Due to the missing convection parameterization, moisture variations along trajectories are lower in the sensitivity experiment, leading to a global median lifetime of 5.62 days, about 0.8 days longer than for the simulation with convection. In the zonal average, differences are most pronounced in tropical and subtropical regions (up to 1.0 days), where the convection scheme is most active, and gradually vanishes toward higher latitudes (Fig. 8b). Comparison of the overall PDF of the uptake times for all detected precipitation events in the three sensitivity experiments shows that all three distributions are similar, and dominated by time scales of less than 4–5 days (Fig. 9a). Actual medians of the LTDs of the three sensitivity experiments [2.9, 3.0, and 3.75 days for the LS16 simulation (black), the results with convection and both free-troposphere and boundary layer uptakes (red), and the sensitivity experiment without convection

Unauthenticated | Downloaded 04/22/25 10:51 AM UTC

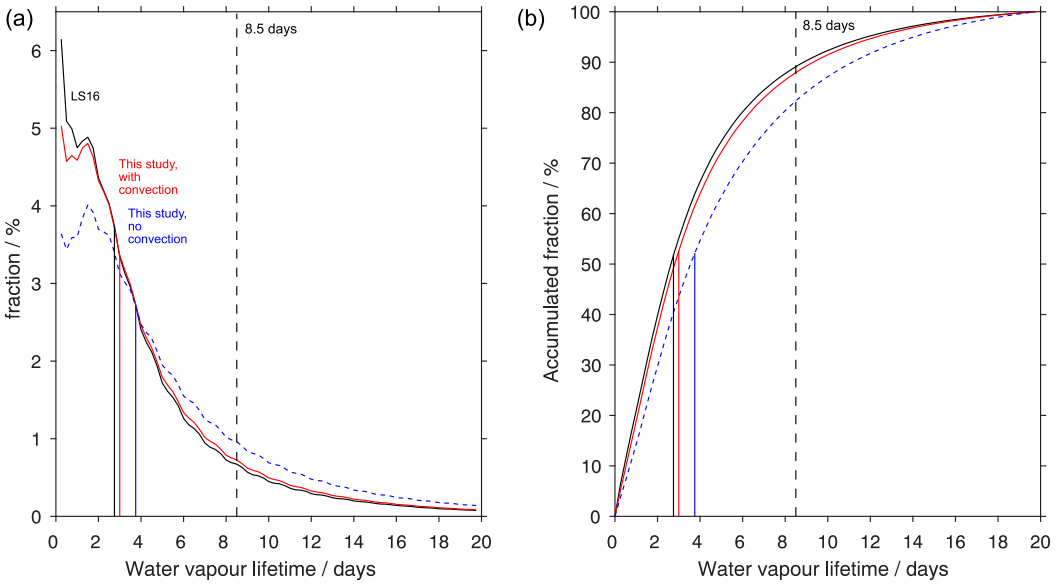


FIG. 9. (a) Probability density function of lifetime diagnosed for all precipitation events from the Lagrangian diagnostic for the year 1993 based on FLEXPART calculations with ERA-Interim data for the lifetime from LS16 with boundary layer uptakes only (black solid) and for both boundary layer and free-troposphere moisture uptakes with convection enabled (red solid) and with convection disabled (blue dashed). (b) Cumulative probability density functions for the three sensitivity experiments. In both panels, the dashed vertical line indicates the global mean turnover time of 8.5 days, and solid vertical lines indicate median values of the respective distribution.

(blue)] are relatively close to the mean values of the distribution. Notably, these LTDs qualitatively resemble the results of VT17 (their Fig. 4), apart from the approximately constant values up to day 2, and a shorter tail in the present results.

The simulation without convection has clear deficiencies when inspecting estimated precipitation in tropical and subtropical latitudes (not shown). The sensitivity simulation can, however, serve as an upper bound for the estimate of the lifetime, while the results of LS16 may serve as a lower bound. In the tropics, one would thus expect median lifetimes of about 4.9 days (4.4 to 5.8 days), in the subtropics about 4.0 days (3.4 to 4.6 days), and in the extratropics about 4.2 days (3.9 to 4.6 days) with a gradual increase to 6.8 days in polar regions. The updated best estimate from LS16 for the global median lifetime of water vapor in the troposphere is $4.8 \pm 0.8$ days, taking into account the uncertainty of the simulation without convection.

These value are markedly different to the turnover time of 8.5 days (Fig. 9b; dashed vertical line), but can be understood by the interpretation of the WaterSip results as being close to the median of the LTD, rather than its mean. As indicated by the vertical lines, the mean global lifetime of 8.5 days would be close to the 85th percentile (here without considering the 5% moisture without known sources), markedly offset from the median as the 50th percentile. A large majority of the water vapor is turned over considerably more quickly than expected from the mean value of a distribution with a long, thin tail. Given the shape of the LTD, the median value thus appears as a more faithful proxy for typical global lifetimes.

Recently, Aemisegger and Papritz (2018) introduced the concept of the strong large-scale oceanic moisture uptakes (SLOEs), defined as significant contributions of evaporation to low-level humidity. SLOEs can be considered as an Eulerian equivalent to the WaterSip diagnostic, working in a Lagrangian framework. The clear correspondence between, for example, the diagnosed moisture sources of Greenland (Sodemann et al. 2008) and Antarctica (Sodemann and Stohl 2009) and SLOE maxima further supports that the moisture source accounting applied in WaterSip provides a robust measure of the LTD, close to its median value.

## 7. Discussion

In the presence of heavily skewed distributions of the lifetime, turnover times cannot be considered as a reliable proxy for age of the large majority of the precipitation in a nonhomogeneous and nonstationarity system, such as the atmosphere. Therefore, the turnover time can neither be expected to faithfully characterize

Unauthenticated | Downloaded 04/22/25 10:51 AM UTC

the LTD at a specific place and time nor inform reliably about its global characteristics. It becomes apparent from this analysis that more sophisticated methods are required to access a larger share of the information contained in the distributions of the atmospheric lifetime of precipitation and of water vapor age. In the following paragraphs, I briefly review existing methods, including their uncertainties, before concluding with potential ways forward in the final section.

### a. *Methods with global and local mass budget calculations*

When turnover times, or depletion time constants are calculated from a mass budget at the grid scale, problems arise in regions with low precipitation. In the subtropics, for example, these local turnover times can exceed values of 30 days (Trenberth 1998; LS16). If horizontal moisture transport is considered during the calculation of gridscale depletion time constants, such high values in the subtropics vanish, and the relative picture of turnover times becomes more consistent with expectations based on prevailing weather systems (LS16). At individual locations and for the global average are still in the range of 8–10 days, mostly due to high values in polar regions. The local calculation of turnover times with or without horizontal fluxes does not explicitly take the processes leading to precipitation formation into account, and the LTD is not accessible from these methods.

The Water Accounting Model (WAM-2layer; van der Ent et al. 2013) is a method that has been used recently to provide an estimate of the global mean lifetime of 8–9 days (van der Ent et al. 2014; VT17). In that method, water transport is calculated based on the water vapor flux on two vertically integrated layers separated at about 200 hPa above surface pressure (based on an empirical formula) to represent the boundary layer and the free troposphere. Tracer moisture originates from grid cells, and is depleted by precipitation. The method then essentially calculates a moisture budget at the gridcell scale as given by an input dataset. Since the method takes into account horizontal transport, the relative patterns of the estimated lifetimes are consistent with the results of LS16. In a case study from West Africa where the atmosphere is characterized by strong vertical shear, the WAM-2layer model was compared to a water vapor tracer simulation with tracer release from a West African catchment (van der Ent et al. 2013). Several aspects of the WAM-2layer method warrant further analysis when working toward an assessment of the atmospheric water cycle from different models. This includes the well-mixed assumption [see discussion in Goessling and Reick (2013)] within the two vertical layers on a gridcell basis, and the sensitivity to model parameters such as the exchange factor between the two layers, the separating height of the two layers, a precipitation process that involves the entire atmospheric column, the use of limiters in the tracer advection, exclusion of polar regions, and the numerical diffusion of the advection scheme. Study setups such as the domain in Guo et al. (2019) could be used in an intercomparison study, for example regarding the spatial range of the moisture source area at a cutoff value of 85% of the total, also in light of the plausibility check using a transport time (section 5). So far, only mean lifetimes have been reported from this method.

### b. *Trajectory-based methods*

Several Lagrangian methods have been applied previously to identify moisture sources, transport and lifetimes. These methods mostly employ backward trajectories of air parcels over a period of typically 5–20 days. A detailed and comprehensive comparison of all aspects of these methods is beyond the scope of this study. Here I briefly touch upon some aspects, that are relevant for future comparison to other lifetime calculations.

The widely used ''moisture recharge'' method (Dirmeyer and Brubaker 1999, 2007) evaluates total column water and evaporation along the track of backward trajectories. Thereby, the contribution of $E$ below the air parcel's position is integrated backward in time along the trajectory until it approaches the column water $W$. Both kinematic and isentropic trajectories have been used with this method. With regard to the present discussion, it is important to note that this method makes use of a well-mixed assumption; that is, it assumes homogeneity of the atmosphere up to the level of the air parcel to allow for transfer of surface evaporation to the air parcel at any vertical position. Violation of the well-mixed assumption could lead to either an overestimate or underestimate of the distance and thus lifetime for this method. The LTD is accessible from this method (VT17, their Fig. 4). Their LTD peaks at below one day and then decays rapidly, with a thin tail that has 95th percentile included after 30 days. Compared to the median of the distribution (5.7 days), this long tail (not related to stratospheric water) results in a substantially higher average lifetime (8.7 days), depending on the chosen cutoff value. In the light of the present study, this again illustrates the point that the mean lifetime is biased toward the long, thin tail. Since the method provides access to the LTD, a detailed comparison to results from other methods is possible.

Another method to identify the source region of water vapor from trajectories is the $E$–$P$ diagnostics by

Unauthenticated | Downloaded 04/22/25 10:51 AM UTC

James et al. (2004) and Stohl and James (2004). This method considers the vertical integral of the moisture budget of individual air parcels at each time step to derive an $E$–$P$ field for the air masses precipitating in a target region. Instead of using the forecast fields $E$ and $P$ from the model, as in the Dirmeyer and Brubaker (1999) method, this method directly identifies changes in specific humidity along an air parcel's trajectory, a variable that is constrained by data assimilation. Rather than providing a lifetime, however, this method requires that the duration of the analysis period be prespecified. Many studies use 10 days to obtain a moisture source pattern, citing the traditional turnover time as a guidance (e.g., Gimeno et al. 2012). Instead of choosing to cut the analysis at the mean turnover time, however, one could argue that it would be more plausible to extend the analysis to 15 or 20 days to avoid underestimating the moisture contributions from more distant regions. In that case, however, the patterns of $E$–$P$ include many distant regions, and become implausible (Stohl et al. 2008), reminiscent to the findings regarding the moisture transport speed (section 5). The discrepancy between choosing a cutoff time at 10 days when the mean turnover time of 8–10 days can be understood considering an expected shape of the LTD. The majority of the precipitation sources would be captured at a cutoff time below 10 days, ignoring the long tail, and resulting in plausible patterns of $E$–$P$.

The Lagrangian moisture source diagnostic by Sodemann et al. (2008), also employed by LS16, and now termed WaterSip (Fremme and Sodemann 2019), provides information on the lifetime of water vapor in the atmosphere based on a moisture budget along backward trajectories. Conceptually based on the $E$–$P$ diagnostics of Stohl and James (2004), the WaterSip method attempts to separate periods of dominating $E$ and $P$ along the transport path of a trajectory. Moisture source information is then obtained from identifying significant moisture increases of an air parcel using a threshold value. A continuous accounting process of the time, location and amount of each contribution and depletion with respect to the current moisture content then yields an estimate of the age of the traced moisture. An important difference to the $E$–$P$ diagnostic is that the WaterSip method identifies how much of the precipitation water has been accounted for (typically 95% or so within 15–20 days; Sodemann and Stohl 2009). Notably, moisture lifetime is obtained without requiring a well-mixed assumption linking surface evaporation to changes at trajectory level. As mentioned above, mixing processes with equally humid or drier air will be missed by that method, which will not allow the method to detect small contributions of long-lived water vapor entering back into the evaporation–precipitation cycle. The work of Dütsch (2016) indicates a potential way to detect such mixing events from the Lagrangian diagnostic. Apart from being partly dependent on threshold values, the method reaches its limits at low humidity levels, such as in high latitudes and at high elevation. As with other Lagrangian methods, interpolation errors can affect diagnosing the net of $E$–$P$, and trajectory calculations in regions dominated by deep convection are uncertain. Tropical precipitation is therefore underrepresented from the LTD. The approximation of immediate rainout of condensed liquid instead of potential reevaporation could in particular impact subtropical lifetimes.

In summary, all available methods have deficiencies, that can be framed with respect to the target quantity LTD, and tested when compared against a ''gold standard'' model, or to suitable observational constraints, if available. Future work will be needed to reduce model deficiencies, and to advance the understanding of different components of the LTD.

## 8. Conclusions and perspectives

Turnover times have long been used as a broad-brush metric to estimate the approximate time on which the atmosphere turns over its water mass. The estimated range of 8–10 days on average has for a long time been used without considering the underlying distribution of lifetimes (LTD). Given the impact of widespread heterogeneity and nonstationarity on water vapor age and lifetime locally and for individual events, the usefulness of such a single metric to assess and compare, for example, the performance of weather prediction and climate models appears limited.

To represent the time scales of the precipitation water in a more balanced way, I propose that using the median of the LTD, instead of the mean value, is substantially more informative. The mean value of a heavily skewed distribution is affected by the very long, thin tail. The substantial uncertainty regarding the length and thickness of the tail of the distribution may be difficult to constrain, depending on the applied method. Questions regarding which part of the tropospheric water cycle could carry tropospheric water vapor on a time scale of several weeks, and how and where it contributes to the precipitation process will need to be addressed in future studies.

In many applications that are related to processes concerning energy and mass transfer, it appears most relevant to use a value that is representative of the majority of the water vapor. The results of the Sodemann et al. (2008) method, used in Laederach and

Unauthenticated | Downloaded 04/22/25 10:51 AM UTC

Sodemann (2016) (LS16) and in the present study, can be (and have been) interpreted in that way. Based on the shape of the LTD, the present study provides the framework to understand the apparent disagreement between LS16 and the mean age obtained from turnover times, and thereby largely resolves the disagreement with VT17.

Based on an update of the results of LS16, and a sensitivity study without parameterized convection in the FLEXPART model, the estimated global *median* lifetime of water vapor from the Lagrangian moisture source diagnostic is 4.8 ± 0.8 days, with substantial variability regarding latitude and region. The water vapor transport distance for a *median* lifetime of about 5 days is more consistent with the spatial scales of typical weather systems than the about 8-day *mean* lifetime obtained from a heavily skewed LTD, and found by the turnover time.

The implications of considering the about 5-day median lifetime rather than the mean of 8–10 days used in previous studies with Lagrangian *E–P* diagnostics of moisture sources of James et al. (2004) may be more limited than one could anticipate. Based on the argument of a 10-day mean lifetime, published studies based on the *E–P* method have commonly chosen a *maximum* lifetime of 10 days as cutoff in their analysis. Since the tail of the LTD is quite thin beyond 10 days, the majority of the contributions should be accounted for when using a 10-day threshold. Nonetheless, further analysis of the implications from this study for such analyses are needed in the future, for example by using locally representative values for the median lifetime.

The variety of methods in use, and their differences, call for a systematic evaluation within a common reference framework. Several studies have applied artificial water tracers to study the lifetime on a global scale (Numaguti 1999; Bosilovich et al. 2005). Building on experiments by Laederach (2016), the recent study by Papritz and Sodemann (2018) demonstrated how a setup with age tracers in a regional model study without parameterized convection can be used to obtain the age of moisture and the lifetime in a specific region (here the northern North Atlantic Ocean basin). Regional models with artificial tracers do not make use of a well-mixed assumption. However, artificial moisture tracers are also affected by model parameterizations and model deficiencies, in particular relating to evaporation, mixing, and microphysics. In situations where moisture advection is essentially limited to a regional model domain, artificial tracer simulations could be used as common reference framework to which or within which several other methods can be compared, similar to van der Ent et al. (2013) and Winschall et al. (2014a).

The lack of direct observations of the moisture age is one of the largest challenges of this field of research. Earliest studies used the half-life of tritium from atmospheric bomb tests to obtain water age in specific cases and regions (von Buttlar and Libby 1955). Instead of a radioactive tracer, which is no longer available, naturally occurring stable isotopes of water vapor could be employed as a tracer variable (e.g., Salati et al. 1979). Temperature-dependent fractionation depletes the water vapor of heavy isotopes compared to an oceanic source. One could expect that longer lifetimes would lead to an overall more depleted atmosphere due to the enhanced probability of condensation and rainout of heavy isotopes (Aggarwal et al. 2012), but with important regional differences. At the same time, mixing with other air masses and cloud microphysics can modify such a general trend. Instead of applying stable isotopes of water with individual methods, it may be more feasible to employ stable water isotopes for verifying the validity of the reference framework. A gold standard method would thus be provided by an evaluation of models equipped with both numerical tracers and stable isotope fractionation processes.

*Acknowledgments.* I gratefully acknowledge ECMWF and MET Norway for making the ERA-Interim data available. Hui Tang pointed me to the similarity with soil organic matter. I am grateful to Stephan Pfahl for comments on an earlier manuscript. I wish to thank Alexander Läderach and colleagues at the University of Bergen, University of Oslo, NILU and University of Stockholm who contributed through valuable discussions to this manuscript. Ruud van der Ent and an anonymous reviewer are acknowledged for comments that helped to substantially improve the manuscript. Part of the computations were performed on resources provided by UNINETT Sigma2—the National Infrastructure for High Performance Computing and Data Storage in Norway.

## REFERENCES

Aemisegger, F., and L. Papritz, 2018: A climatology of strong large-scale ocean evaporation events. Part I: Identification, global distribution, and associated climate conditions. *J. Climate*, **31**, 7287–7312, https://doi.org/10.1175/JCLI-D-17-0591.1.

Aggarwal, P. K., O. A. Alduchov, K. O. Froehlich, L. J. Araguas-Araguas, N. C. Sturchio, and N. Kurita, 2012: Stable isotopes in global precipitation: A unified interpretation based on atmospheric moisture residence time. *Geophys. Res. Lett.*, **39**, L11705, https://doi.org/10.1029/2012GL051937.

Bosilovich, M. G., S. D. Schubert, and G. K. Walker, 2005: Global changes of the water cycle intensity. *J. Climate*, **18**, 1591–1608, https://doi.org/10.1175/JCLI3357.1.

Unauthenticated | Downloaded 04/22/25 10:51 AM UTC

Cayan, D. R., 1992: Latent and sensible heat-flux anomalies over the northern oceans: The connection to monthly atmospheric circulation. *J. Climate*, **5**, 354–369, https://doi.org/10.1175/1520-0442(1992)005<0354:LASHFA>2.0.CO;2.

Dee, D. P., and Coauthors, 2011: The ERA-Interim reanalysis: Configuration and performance of the data assimilation system. *Quart. J. Roy. Meteor. Soc.*, **137**, 553–597, https://doi.org/10.1002/qj.828.

Dettmann, E. H., 2013: Turnover time. *Encyclopedia of Ecology*, Elsevier, 503–508.

Dirmeyer, P. A., and K. L. Brubaker, 1999: Contrasting evaporative moisture sources during the drought of 1988 and the flood of 1993. *J. Geophys. Res.*, **104**, 19 383–19 397, https://doi.org/10.1029/1999JD900222.

——, and ——, 2007: Characterization of the global hydrologic cycle from a back-trajectory analysis of atmospheric water vapor. *J. Hydrometeor.*, **8**, 20–37, https://doi.org/10.1175/JHM557.1.

Dütsch, M. L., 2016: Stable water isotope fractionation processes in weather systems and their influence on isotopic variability on different time scales. Ph.D. thesis, ETH Zürich, 159 pp., https://doi.org/10.3929/ethz-b-000000058.

Fremme, A., and H. Sodemann, 2019: The role of land and ocean evaporation on the variability of precipitation in the Yangtze River valley. *Hydrol. Earth Syst. Sci.*, **23**, 2525–2540, https://doi.org/10.5194/hess-23-2525-2019.

Gimeno, L., and Coauthors, 2012: Oceanic and terrestrial sources of continental precipitation. *Rev. Geophys.*, **50**, RG4003, https://doi.org/10.1029/2012RG000389.

Goessling, H. F., and C. H. Reick, 2013: On the "well-mixed" assumption and numerical 2-D tracing of atmospheric moisture. *Atmos. Chem. Phys.*, **13**, 5567–5585, https://doi.org/10.5194/acp-13-5567-2013.

Guo, L., R. J. van der Ent, N. P. Klingaman, M.-E. Demory, P. L. Vidale, A. G. Turner, C. C. Stephan, and A. Chevuturi, 2019: Moisture sources for East Asian precipitation: Mean seasonal cycle and interannual variability. *J. Hydrometeor.*, **20**, 657–672, https://doi.org/10.1175/JHM-D-18-0188.1.

Held, I. M., and B. J. Soden, 2006: Robust responses of the hydrological cycle to global warming. *J. Climate*, **19**, 5686–5699, https://doi.org/10.1175/JCLI3990.1.

Hodnebroug, and Coauthors, 2019:Increased water vapor lifetime due to global warming. *Atmos. Chem. Phys.*, **19**, 12 887–12 899, https://doi.org/10.5194/acp-19-12887-2019.

James, P., A. Stohl, N. Spichtinger, S. Eckhardt, and C. Forster, 2004: Climatological aspects of the extreme European rainfall of August 2002 and a trajectory method for estimating the associated evaporative source regions. *Nat. Hazards Earth Syst. Sci.*, **4**, 733–746, https://doi.org/10.5194/nhess-4-733-2004.

Knippertz, P., and H. Wernli, 2010: A Lagrangian climatology of tropical moisture exports to the Northern Hemispheric extratropics. *J. Climate*, **23**, 987–1003, https://doi.org/10.1175/2009JCLI3333.1.

Laederach, A., 2016: Characteristic scales of atmospheric moisture transport. Ph.D. thesis, ETH Zurich, 143 pp., https://doi.org/10.3929/ethz-a-010741025.

——, and H. Sodemann, 2016: A revised picture of the atmospheric residence time of water vapor. *Geophys. Res. Lett.*, **121**, 3040–3061, https://doi.org/10.1002/2015GL067449.

McGuire, K. J., and J. J. McDonnell, 2006: A review and evaluation of catchment transit time modeling. *J. Hydrol.*, **330**, 543–563, https://doi.org/10.1016/j.jhydrol.2006.04.020.

Numaguti, A., 1999: Origin and recycling processes of precipitating water over the Eurasian continent: Experiments using an atmospheric general circulation model. *J. Geophys. Res.*, **104**, 1957–1972, https://doi.org/10.1029/1998JD200026.

Papritz, L., and H. Sodemann, 2018: Characterizing the local and intense water cycle during a cold air outbreak in the Nordic seas. *Mon. Wea. Rev.*, **146**, 3567–3588, https://doi.org/10.1175/MWR-D-18-0172.1.

——, S. Pfahl, I. Rudeva, I. Simmonds, H. Sodemann, and H. Wernli, 2014: The role of extratropical cyclones and fronts for Southern Ocean freshwater fluxes. *J. Climate*, **27**, 6205–6224, https://doi.org/10.1175/JCLI-D-13-00409.1.

Peixóto, J., and A. Oort, 1983: The atmospheric branch of the hydrological cycle and climate. *Variations in the Global Water Budget*, A. Street-Perrott, M. Beran, and R. Ratcliffe, Eds., Springer, 5–65, https://doi.org/10.1007/978-94-009-6954-4_2.

Persson, P. O. G., J. E. Hare, C. W. Fairall, and W. D. Otto, 2005: Air–sea interaction processes in warm and cold sectors of extratropical cyclonic storms observed during FASTEX. *Quart. J. Roy. Meteor. Soc.*, **131**, 877–912, https://doi.org/10.1256/qj.03.181.

Ralph, F. M., P. J. Neiman, G. N. Kiladis, K. Weickmann, and D. W. Reynolds, 2011: A multiscale observational case study of a Pacific atmospheric river exhibiting tropical–extratropical connections and a mesoscale frontal wave. *Mon. Wea. Rev.*, **139**, 1169–1189, https://doi.org/10.1175/2010MWR3596.1.

Salati, E., A. Dall'Olio, E. Matusi, and J. R. Gat, 1979: Recycling of water in the Amazon basin: An isotropic study. *Water Resour. Res.*, **15**, 1250–1258, https://doi.org/10.1029/WR015i005p01250.

Sodemann, H., and A. Stohl, 2009: Asymmetries in the moisture origin of Antarctic precipitation. *Geophys. Res. Lett.*, **36**, L22803, https://doi.org/10.1029/2009GL040242.

——, and ——, 2013: Moisture origin and meridional transport in atmospheric rivers and their association with multiple cyclones. *Mon. Wea. Rev.*, **141**, 2850–2868, https://doi.org/10.1175/MWR-D-12-00256.1.

——, C. Schwierz, and H. Wernli, 2008: Interannual variability of Greenland winter precipitation sources: Lagrangian moisture diagnostic and North Atlantic Oscillation influence. *J. Geophys. Res.*, **113**, D03107, https://doi.org/10.1029/2007JD008503.

Stohl, A., and P. James, 2004: A Lagrangian analysis of the atmospheric branch of the global water cycle. Part I: Method description, validation, and demonstration for the August 2002 flooding in central Europe. *J. Hydrometeor.*, **5**, 656–678, https://doi.org/10.1175/1525-7541(2004)005<0656:ALAOTA>2.0.CO;2.

——, C. Forster, A. Frank, P. Seibert, and G. Wotawa, 2005: Technical note: The Lagrangian particle dispersion model FLEXPART version 6.2. *Atmos. Chem. Phys.*, **5**, 2461–2474, https://doi.org/10.5194/acp-5-2461-2005.

——, ——, and H. Sodemann, 2008: Remote sources of water vapor forming precipitation on the Norwegian west coast at 60°N—A tale of hurricanes and an atmospheric river. *J. Geophys. Res.*, **113**, D05102, https://doi.org/10.1029/2007JD009006.

Trenberth, K. E., 1998: Atmospheric moisture residence times and cycling: Implications for rainfall rates and climate change. *Climatic Change*, **39**, 667–694, https://doi.org/10.1023/A:1005319109110.

——, 2011: Changes in precipitation with climate change. *Climate Res.*, **47**, 123–138, https://doi.org/10.3354/cr00953.

Unauthenticated | Downloaded 04/22/25 10:51 AM UTC

Trumbore, S., 2000: Age of soil organic matter and soil respiration: Radiocarbon constraints on belowground C dynamics. *Ecol. Appl.*, **10**, 399–411, https://doi.org/10.1890/1051-0761(2000)010[0399:AOSOMA]2.0.CO;2.

van der Ent, R. J., and O. A. Tuinenbourg, 2017: The residence time of water in the atmosphere revisited. *Hydrol. Earth Syst. Sci.*, **21**, 779–790, https://doi.org/10.5194/hess-21-779-2017.

——, ——, H. R. Knoche, H. Kunstmann, and H. H. G. Savenije, 2013: Should we use a simple or complex model for moisture recycling and atmospheric moisture tracking? *Hydrol. Earth Syst. Sci.*, **17**, 4869–4884, https://doi.org/10.5194/hess-17-4869-2013.

——, L. Wang-Erlandsson, P. W. Keys, and H. H. G. Savenije, 2014: Contrasting roles of interception and transpiration in the hydrological cycle—Part 2: Moisture recycling. *Earth Syst. Dyn.*, **5**, 471–489, https://doi.org/10.5194/esd-5-471-2014.

von Buttlar, H., and W. Libby, 1955: Natural distribution of cosmic-ray produced tritium. II. *J. Inorg. Nucl. Chem.*, **1**, 75–91, https://doi.org/10.1016/0022-1902(55)80070-X.

Winschall, A., S. Pfahl, H. Sodemann, and H. Wernli, 2014a: Comparison of Eulerian and Lagrangian moisture source diagnostics—The flood event in eastern Europe in May 2010. *Atmos. Chem. Phys.*, **14**, 6605–6619, https://doi.org/10.5194/acp-14-6605-2014.

——, H. Sodemann, and S. Pfahl, 2014b: How important is intensified evaporation for Mediterranean precipitation extremes? *J. Geophys. Res. Atmos.*, **119**, 5240–5256, https://doi.org/10.1002/2013JD021175.

Unauthenticated | Downloaded 04/22/25 10:51 AM UTC